REALISTIC FEA MODELING OF 3D WOVEN COMPOSITES ON MESOSCALE

A. Drach[1], B. Drach[2], I. Tsukrov[1]*, H. Bayraktar[3], J. Goering[3]
[1] Mechanical Engineering, University of New Hampshire, Durham, NH, USA
[2] Mechanical & Aerospace Engineering, New Mexico State University, Las Cruces, NM, USA
[3] Albany Engineered Composites, Rochester, NH, USA
* Corresponding author (igor.tsukrov@unh.edu)

Keywords: *3D woven composite, mesoscale, matrix microcracking, curing*

Abstract

Mesoscale modeling of three-dimensional woven composites presents significant challenges related to accurate representation of as-woven geometry of the reinforcement [1]. There are two approaches most commonly used to define the geometry of reinforcement. One is based on the nominal description of composite, and the other one involves fabric mechanics simulations. In our previous publications, we attempted to evaluate the efficiency and accuracy of these two approaches for prediction of the overall elastic properties and residual stresses due to curing for the so-called ply-to-ply reinforcement architecture, see [2].
In this paper, we present a straightforward procedure to develop realistic finite element models of unit cells for 3D woven composites based on the as-woven reinforcement geometry obtained by the textile modeling software DFMA [3]. We consider two configurations of an orthogonally reinforced composite and describe all steps of the model development. Numerical simulations to predict the overall elastic moduli and evaluate the materials' potential to develop high residual stresses due to curing are described.

1 Introduction

On the mesoscale, the structure of woven composites can be described as a dual-phase system consisting of the bundles of fibers (yarns or tows) embedded in the matrix, as illustrated in Fig. 1. The smallest repeating portion of the composite is called a unit cell (UC), see Fig. 2. Interaction of the UC with the surrounding material is modeled by assigning periodic boundary conditions which require that boundaries of the UC deform in a way that preserves the continuity of the composite. At the microscale, yarns consist of several thousands of individual fibers (Fig. 1).

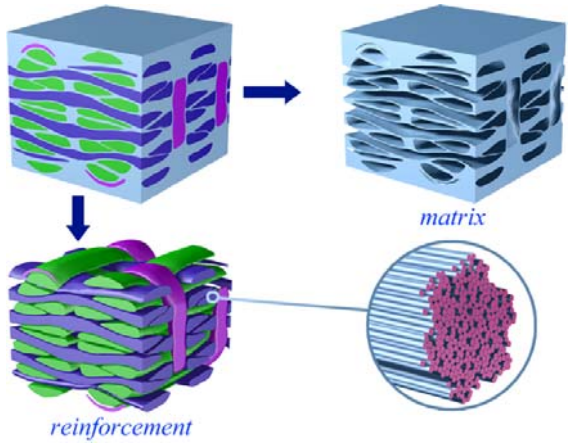

Fig. 1. Material structure of 3D woven composites on meso- and microscale

Depending on the direction of reinforcement within a UC, the yarns are identified as longitudinal (warp), transverse (weft) and through-thickness (binder). The configuration illustrated in Fig. 1 is the so-called 1x1 orthogonal architecture. This configuration is characterized by the binder yarns going vertically (up or down) through the entire thickness of the composite at each crossing with the weft yarns column. The 2x2 orthogonal architecture is similar to the 1x1, but the binder yarns go through the thickness at every other crossing.

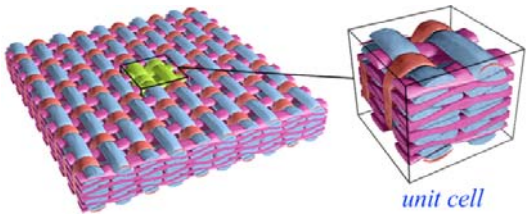

Fig. 2. Unit cell of a 3D woven composite

We use these two orthogonal architectures (1x1 and 2x2) to present a procedure for construction of realistic finite element (FE) models of 3D woven composites on mesoscale. Usually, such models are developed based on the nominal geometry of composites. They are constructed from the weaving pattern with a chosen shape of yarn cross-sections. This approach has been extensively discussed in the literature [4,5] and implemented in such software packages as TexGen, WiseTex, DYNAFAB, ScotWeave, etc. Another class of approaches is based on the volumetric subdivisions known as "mosaic" models [6,7]. The relative ease of nominal geometry model preparation, however, introduces some limitations to this approach. The architectures with a large volume fraction of reinforcements or a large number of binder yarns are difficult to model due to the inability of this approach to automatically account for the deformations of yarn cross-sections during manufacturing. This leads to the geometric incompatibility problem which is manifested by the interpenetration of yarn cross-sections. Several authors [1,8,9] have developed remedial procedures including semi-automatic deformations of the yarn shapes, reductions of their cross-sectional area, and special procedures to prescribe changes in cross-sectional area and/or axial rotation of the yarn. However, even for the geometries that can be modeled successfully, the artificially prescribed shape of the cross-section does not provide an accurate description of the actual microstructure as observed in the micrographs, see for example [10]. The actual geometry deviates from a nominal one due to the effect of tensile and contact pressure forces during the weaving process.

Some limitations of the "nominal geometry" approach can be addressed by utilizing the more realistic as-woven geometry of reinforcement. However, reproduction of as-woven geometry requires complicated textile mechanics simulations. An approach developed by Wang et al. [3,11,12] is based on the so-called "multi-chain digital element analysis". The yarns are represented as bundles of digital elements which are modeled as a series of interconnected rods (similar to FE truss elements), see Fig. 3. To obtain the as-woven geometry, deformation of the yarns is modeled as a step-by-step process of applying the tension forces to the yarns, subdividing the yarns in more digital elements and relaxing the stresses. The contact is simulated by the special contact elements. This approach is implemented in the Digital Fabric Mechanics Analyzer (DFMA, fabricmechanics.com) software by the original authors of the method. The output of the simulation results is organized as reinforcement surface mesh (STL format) or point cloud data.

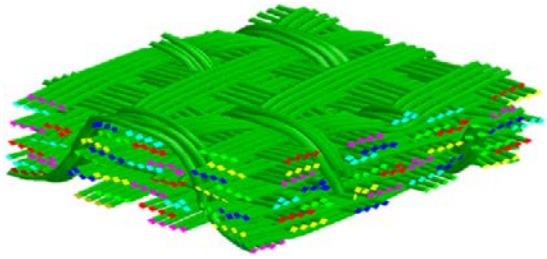

Fig. 3. DFMA model of 2x2 orthogonal weave (intermediate configuration with 4 digital elements per yarn)

Our procedure for development of mesoscale FE models for 3D woven composites is based on the as-woven geometry presented as point cloud data. Section 2 discusses the preprocessing of geometric data, corrections of the geometrical errors, and development of the FE mesh. Section 3 deals with assigning material properties, boundary conditions, and selection of the solvers for finite element simulations. Section 4 provides predictions for effective elastic properties of two considered reinforcement configurations. In Section 5 we evaluate the potential of the 3D woven composites to microcrack during resin curing by considering the stresses, caused by mismatch in coefficients of thermal expansion (CTEs) between resin and fibers, when the material cools from curing to room temperature.

2 Development of FE Meshes on Mesoscale

Initial woven geometry of the yarns was exported from DFMA software (see [3]) in GEO format. The format contains coordinates of points defining the reinforcement yarns ("point clouds"). The point clouds are organized in sets of cross-sectional profiles of each yarn.

Yarn extension to form UC

One of the problems with generation of the UC models from DFMA output data is that the yarn end caps in the unit cell are not parallel to the UC boundaries, therefore some of the yarns do not reach the boundaries of UC. To deal with the issue, we make use of the yarn periodicity conditions

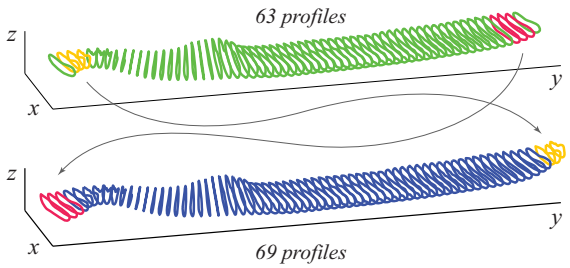

Fig. 4. Illustration of yarn extension procedure based on the duplication of a specified number of profiles and addition of them to the beginning and end of the yarns.

implemented in DFMA: the first and the last profiles of yarn's final geometry are of the same shape and orientation. This allows for extensions of yarns to the boundaries of UC. A Python script was written to extend the yarns in both directions. This is done by duplicating a specified number of profiles and adding them to the beginning and end of the yarn. Fig. 4 shows the yarn extension by three profiles in each direction (closed loops represent yarn profiles). The number of extension profiles is chosen so that all end profiles' points lie outside of the unit cell dimensions. Later the excessive yarn elements are cut off to form flat unit cell surfaces.

The extended yarns are then processed in open source software package MeshLab (meshlab. sourceforge.net) to convert point clouds to triangular surface meshes using Ball Pivoting Surface Reconstruction algorithm. The triangular surface meshes of the individual yarns are saved in STL format.

It is important to check whether periodicity of the yarn geometry is satisfied. In some woven configurations, yarns protrude beyond the dimensions of UC both longitudinally and transversely. Since only one copy of each yarn in the UC is exported from DFMA software, it may be needed to duplicate some yarns to the opposite sides of UC to ensure the shape periodicity after the model is cut to the UC dimensions.

Yarn interpenetration correction

The geometric models generated by utilizing DFMA and some other reinforcement modeling techniques often contain yarn interpenetrations (portions of two yarns occupying the same volume in space). Any instance of two surface elements penetrating each other results in an error during meshing with volume elements. Several ways of dealing with this problem have been proposed in the literature including semi-automatic yarn deformation simulations [1], manual manipulations (rotations and shape changes) of portions of the yarns [8,9], and model-wide reductions of yarn cross-section areas [4]. The first method involves subdivision of the UC into portions, each containing only one instance of interpenetration between two yarns and then shifting and deforming interpenetrating portions of the yarns. This method may be difficult to implement for the cases of interpenetrations of several adjacent yarns due to the limitation of repair of two yarns at a time. This can lead to the lockup of solution because each repair affects another interpenetration instance and does not allow treating all interpenetrations of a yarn simultaneously. The second method requires extensive manual processing and may result in unrealistic topologies. The third method may lead to a significant loss of reinforcement volume fraction.

The approach to deal with the local yarn interpenetration utilized in this paper is based on the element-wise penetration detection and correction by moving the vertices of the penetrating element outside of the penetration zone. Two types of penetrations were observed in the considered models: "vertex inside element" and "edge inside element" (Fig. 5).

Penetration correction is performed in two steps and is implemented in a custom MATLAB code. In the first step, the "vertex inside element" type penetrations are identified and corrected as follows. The algorithm goes through every element in the host yarn (yarn whose interior is checked for the presence of penetrating vertices) and checks if any vertices of potentially penetrating yarns are inside the host yarn element. The vertex is considered to be inside the element if it is inside the triangular prism built from the host element protruding in the direction

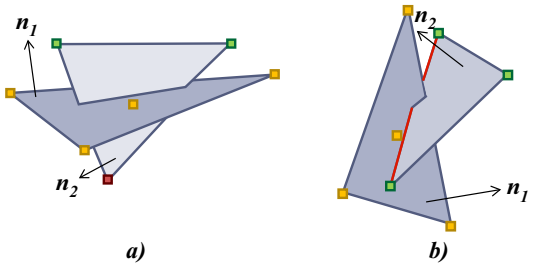

Fig. 5. Two types of element interpenetration observed in the models: a) vertex inside element b) edge inside element

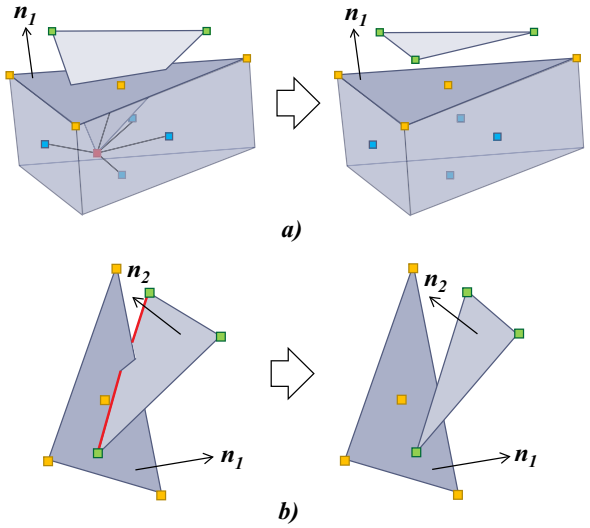

Fig. 6. Schematics of identification and correction of the two types of element interpenetration

opposite to its external normal vector n_1 (see Fig. 6a). In this case the vectors connecting the vertex with the centers of the prism sides are all within 90 degrees of the corresponding sides' internal normal vectors. If a vertex is found to be inside the host element, it is moved in the direction of host element's normal until a minimum specified distance between the vertex and the element is established. The movement of the vertices is stopped if a potential intersection with other elements of the penetrating yarn is detected ("self-penetration" check).

In the second step, the "edge inside element" type penetrations are identified and corrected if any are left after the first step. The MATLAB code goes through every element of the host yarn and checks if any of the edges of the potentially penetrating yarn elements intersect the host element via ray/triangle intersection check. Fast implementation of the intersection check algorithm is given in [13]. If any edges are found to intersect the host element, the vertices comprising the edge are moved along the host element external normal until a minimum specified distance between the vertices and the host element is reached.

In both steps, the algorithms are dependent on several parameters including height of the prism, distance searched for potentially penetrating vertices and edges, *etc*. All of these parameters need to be tuned for successful penetration correction. Note that a different method to repair interpenetrations based on the voxel representation of the reinforcement is proposed by the authors in [14].

Meshing of UC

As discussed above, the yarns are extended to protrude beyond UC dimensions to ensure shape periodicity on the opposite sides. After all penetrations are eliminated, the yarns need to be cut to the final UC dimensions. For meshes with a small number of elements, this can be achieved using SolidWorks or various FE preprocessors. However for models with large numbers of elements (in our case, more than 250,000) the use of the general purpose commercial packages becomes inefficient. The authors developed a MATLAB script that goes through every element intersected by the cutting planes (planes parallel to XZ and YZ coordinate planes located at the coordinates corresponding to the dimensions of the UC), determines the points of intersection, and creates new elements based on these and old points.

Cutting of triangular elements to UC boundaries produces new elements, some of which are of bad aspect ratios and some even have zero areas. Such elements need to be eliminated before proceeding to meshing with 3D elements. This is achieved by using "MeshOnMesh" function in MSC Patran. This step produces uniform mesh that does not contain skewed elements. At the same time, this function allows for flexible adjustment of mesh discretization which is useful for mesh sensitivity studies. The final step before volumetric meshing involves closing the volume of the yarn surface meshes and generating conforming surface mesh of the matrix. For this step, free edges of the yarn mesh are extracted and used to create yarn end caps and matrix boundaries. The final surface meshes of 1x1 and 2x2 orthogonal yarn configurations without matrices are shown in Fig. 7. Meshing of these surfaces with tetrahedral linear elements has been performed in MSC Patran (see Table 1 for details on the final 3D meshes).

The meshes are imported into MSC Mentat which is the graphical pre- and post-processor for MSC Marc FE solver. During the import stage, the reinforcement and matrix meshes are processed separately to preserve the topological features in the unit cell. Each yarn is imported as a separate set of 3D finite elements, allowing to distinguish them in

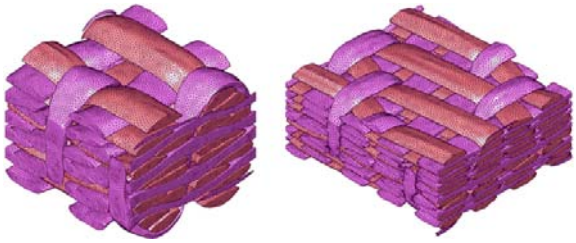

(a) (b)

Fig. 7. Two woven reinforcement configurations: (a) 1x1 orthogonal and (b) 2x2 orthogonal

Table 1. Details of unit cell meshes

	1x1 ortho	**2x2 ortho**
# of elements	1,701,378	1,877,323
# of nodes	295,456	322,377

the model and during the post-processing of results. The matrix mesh is imported as a single element set.

3 Model Preparation and Implementation

Periodic boundary conditions

The obtained FEA models of unit cells are periodic in warp and weft directions, and represent the full height of the composite in the through-thickness direction. To account for the periodicity, servo link option is used in MSC Marc to create the following nodal ties between the opposite faces of the unit cell in weft and warp directions:

$$\underline{u}_i^+ = \underline{u}_i^- + \delta_i \quad (i = x, y) \qquad (1)$$

where $\underline{u}_i^+$ and $\underline{u}_i^-$ are the nodal displacements on the positive and negative faces, respectively; δ_i is the average displacement in the i-th direction; and x and y are the warp and weft directions, correspondingly.

Material properties of constituents

There are two material phases designated in our mesoscale models: matrix and reinforcing yarns. The matrix phase is RTM6 epoxy with parameters $E^{(m)} = 2.9GPa$, $\nu^{(m)} = 0.3$, $\alpha^{(m)} = 6 \cdot 10^{-5} 1/K$. The reinforcement phase consists of resin impregnated 12K carbon yarns (12,000 fibers per yarn) with 80% volume fraction of fibers within the yarns. Utilizing Hashin's and Schapery's [15–18] micromechanical formulas for unidirectional fiber bundles, the following effective properties of the impregnated yarns are obtained [2]: $E_1^{(t)} = 221.4GPa$, $E_2^{(t)} = 12.6GPa$, $G_{12}^{(t)} = 7.4GPa$, $\nu_{12}^{(t)} = 0.34$, $\nu_{23}^{(t)} = 0.32$, $a_1^{(t)} = -2.5 \cdot 10^{-7} 1/K$, $a_2^{(t)} = 1.7 \cdot 10^{-5} 1/K$. Hereafter, E, G, ν and α are the Young's modulus, shear modulus, Poisson's ratio and thermal expansion coefficient correspondingly; direction *1* is longitudinal (yarn direction), and directions *2* and *3* are transverse. The yarn volume fraction in both models is approximately 0.65.

Material orientations within yarns

The reinforcement material is anisotropic, so the material orientations have to be defined. Material orientation defines the direction of the principal material axes in the element relative to the global coordinate system of the FE mesh.

In our procedure, this information is derived from the point cloud data imported from DFMA (see Section 2). In addition to the yarn profile outlines, DFMA output also contains the center points for each of the yarn profiles. These points are consecutively connected into a piecewise linear curve (polyline). The major principal axis for each of the yarn elements is assumed to be coincident with the nearest segment of this polyline (see Fig. 8). The second principal axis is taken in radial direction from the center line to the centroid of the element. The third principal direction is defined as the vector product of the first two.

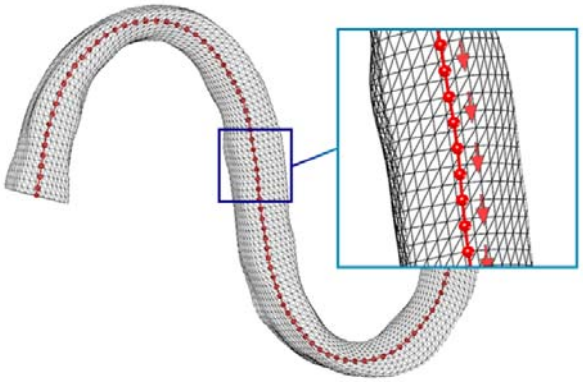

Fig. 8. Assignment of the material orientations for a yarn based on the connected center points

Analysis settings

Four linear simulations for each of the constructed models were conducted as described in Sections 4 and 5. They were performed in MSC Marc software and took approximately 3 minutes each on a workstation with Intel i7-3770 4-core processor and 32GB of RAM.

Each simulation was run as a separate job in MSC Marc. The job parameters were set as follows: residuals and displacements convergence criteria with tolerance of 10^{-4}, iterative matrix solver with tolerance of 10^{-6}, four manually prescribed parallelization domains. It is interesting to note that only few of many available options for matrix solvers allowed to successfully and reasonably quickly perform the simulations. For example, the default solver option (multifrontal direct sparse) required 8x more CPU time to provide the solution than the iterative solvers. Another direct solver (PARDISO) performed reasonably fast, however, required 5x more RAM memory. The default iterative solver (CASI iterative) was not suitable for these simulations, because it would not converge regardless of the choice of user-defined parameters. A short study was performed in effort to identify the cause for such a strong dependence on the choice of solver. It was found that neither the implementation of boundary/periodic conditions, nor the mesh discretization caused this issue. However, the modification of material properties (reducing the contrast in stiffness between constituents) allowed to alleviate this issue, indicating that strong anisotropy of reinforcement together with its complex distribution in space and sharp gradients at the matrix/reinforcement interface could be the major causes for such numerical instabilities.

4 Effective elastic properties

Predictions of the overall elastic moduli of the composite were found by evaluating its response to the applied strain fields. Three loadcases were applied to each of the unit cell models to calculate Young's moduli and Poisson's ratios (shear loading response is not reported in this paper).

Each loadcase was setup to satisfy the periodicity conditions on the in-plane faces of a unit cell, while the uniaxial strains were applied in x, y and z directions consecutively.

Table 2. Effective elastic properties of the considered 3D woven composites

	E_x, GPa	E_y, GPa	E_z, GPa	ν_{xy}	ν_{xz}	ν_{yz}
1x1	54.4	49.9	7.98	0.06	0.47	0.56
2x2	54.0	69.2	7.54	0.05	0.53	0.47

The obtained overall moduli are presented in Table 2 (direction x is warp, direction y is weft, and z is through-thickness).

5 Predictions of residual stresses due to cure

To estimate the cure-induced stresses in the composite, we modeled the curing process as a uniform drop in temperature from the resin curing temperature of 160˚C to room temperature of 20˚C. With this simplified analysis we found distributions of the residual stress caused by the difference in CTEs between yarns and pure matrix material. The so-called parabolic stress (see, for example, [10,19]) was used to compare susceptibility of various reinforcement architectures to matrix microcracking:

$$\sigma_{PAR} = \begin{cases} \sqrt{\sigma_{VM}^2 + A \cdot \sigma_H} & \text{if } \left(\sigma_{VM}^2 + A \cdot \sigma_H\right) \geq 0 \\ 0 & \text{otherwise} \end{cases} \quad (2)$$

where σ_{VM} is the equivalent (von Mises) deviatoric stress, σ_H is the hydrostatic stress, and A is the material constant found from tests of the neat resin. The parabolic stress was calculated during the post-processing of modeling results (stress tensor components output) in MATLAB. In [19] this constant was determined for numerical modeling of unidirectional carbon/epoxy composites from uniaxial tensile and torsion tests.

Fig. 9 provides distribution of the residual parabolic stress σ_{PAR} in the resin. The curve for each material shows the percentage of matrix volume with σ_{PAR} lower than the value indicated at the abscissa axis. It can be seen that even though the overall distribution of parabolic stresses is similar in the tails (lower 10% and upper 5%), the range in-between shows significant differences. The magnitude of the stress grows much faster from 90 to 120 *MPa* in the 1x1 reinforcement compared to the 2x2 architecture. This suggests that under similar conditions, the 3D woven composite with 1x1 architecture will have larger pockets with elevated levels of cure-induced

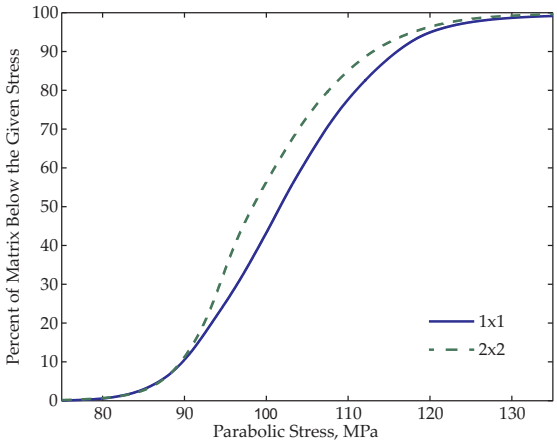

Fig. 9. Distribution of residual parabolic stresses in the matrix material for 1x1 and 2x2 orthogonal reinforcement architectures

stresses in the matrix, making this architecture more susceptible to the manufacturing-induced cracking during the curing process. This observation is consistent with the experimental data reported previously in [10].

6 Conclusions

Realistic FEA models of 3D woven composites on the mesoscale are constructed using data from the fabric mechanics simulation software. The unit cell model development includes extension of the yarns, correction of yarn interpenetrations, and assignment of material orientations and proper boundary conditions. The developed models are successfully used to predict effective elastic properties of the composites and evaluate their potential to develop high residual stresses due to curing.

Acknowledgements

This material is based upon work supported by the National Science Foundation under Grant No. CMMI-1100409. This collaborative research was also supported by Albany Engineered Composites, Inc. and the New Hampshire Innovation Research Center.

References

[1] Lomov S., Ivanov D., Verpoest I., Zako M., Kurashiki T., Nakai H., and Hirosawa S., 2007, "Meso-FE modelling of textile composites: Road map, data flow and algorithms," Composites Science and Technology, **67**(9), pp. 1870–1891.

[2] Tsukrov I., Giovinazzo M., Vyshenska K., Bayraktar H., Goering J., and Gross T., 2012, "Comparison of two approaches to model cure-induced microcracking in three-dimensional woven composites," Proceedings of the 2012 International Mechanical Engineering Congress & Exposition (IMECE2012), Houston, TX, pp. 1–6.

[3] Miao Y., Zhou E., Wang Y., and Cheeseman B., 2008, "Mechanics of textile composites: Micro-geometry," Composites Science and Technology, **68**(7-8), pp. 1671–1678.

[4] Lin H., Brown L. P., and Long A. C., 2011, "Modelling and Simulating Textile Structures Using TexGen," Advanced Materials Research, **331**, pp. 44–47.

[5] Verpoest I., and Lomov S., 2005, "Virtual textile composites software WiseTex: Integration with micro-mechanical, permeability and structural analysis," Composites Science and Technology, **65**(15-16), pp. 2563–2574.

[6] Tong L., Mouritz A. P., and Bannister M. K., 2002, 3D Fibre Reinforced Polymer Composites, Elsevier.

[7] Bogdanovich A. E., 2006, "Multi-scale modeling, stress and failure analyses of 3-D woven composites," Journal of Materials Science, **41**(20), pp. 6547–6590.

[8] Sherburn M., 2007, "Geometric and Mechanical Modelling of Textiles. PhD Dissertation," University of Nottingham.

[9] Rinaldi R. G., Blacklock M., Bale H., Begley M. R., and Cox B. N., 2012, “Generating virtual textile composite specimens using statistical data from micro-computed tomography: 3D tow representations,” Journal of the Mechanics and Physics of Solids, **60**(8), pp. 1561–1581.

[10] Tsukrov I., Bayraktar H., Giovinazzo M., Goering J., Gross T., Fruscello M., and Martinsson L., 2011, “Finite Element Modeling to Predict Cure-Induced Microcracking in Three-Dimensional Woven Composites,” International Journal of Fracture, **172**(2), pp. 209–216.

[11] Wang Y., and Sun X., 2001, “Digital-element simulation of textile processes,” Composites Science and Technology, **61**(2), pp. 311–319.

[12] Zhou G., Sun X., and Wang Y., 2004, “Multi-chain digital element analysis in textile mechanics,” Composites Science and Technology, **64**(2), pp. 239–244.

[13] Möller T., and Trumbore B., 1997, “Fast, minimum storage ray-triangle intersection,” Journal of graphics tools, (1), pp. 1–7.

[14] Drach A., Drach B., and Tsukrov I., “Processing of fiber architecture data for finite element modeling of 3D woven composites,” Advances in Engineering Software, **in press**.

[15] Hashin Z., and Rosen B. W., 1964, “The Elastic Moduli of Fiber-Reinforced Materials,” Journal of Applied Mechanics, **31**, pp. 223–232.

[16] Hashin Z., 1983, “Analysis of composite materials: A survey,” Journal of Applied Mechanics, **50**, pp. 481–505.

[17] Schapery R. A., 1968, “Thermal Expansion Coefficients of Composite Materials Based on Energy Principles,” Journal of Composite Materials, **2**(3), pp. 380–404.

[18] Tsukrov I., Drach B., and Gross T. S., 2012, “Effective stiffness and thermal expansion coefficients of unidirectional composites with fibers surrounded by cylindrically orthotropic matrix layers,” International Journal of Engineering Science, **58**, pp. 129–143.

[19] Hobbiebrunken T., Hojo M., Fiedler B., Tanaka M., Ochiai S., and Schulte K., 2004, “Thermomechanical Analysis of Micromechanical Formation of Residual Stresses and Initial Matrix Failure in CFRP,” JSME International Journal Series A, **47**(3), pp. 349–356.